Journal of Extracellular Vesicles

RESEARCH ARTICLE OPEN ACCESS

Proteomic Profiling of Human Extracellular Vesicles Reveals Diagnostic Biomarkers for Colon Adenocarcinoma

Yura Seo[1,2] | Yoon Dae Han[3] | Linda Bojmar[4,5] | Kyung-A Kim[1,2] | Yurin Seo[1,2] | Taeyul K. Kim[1,2] | Suho Lee[1,2] | Yeleem Kim[1,2] | Hye Bin Choi[1] | Yujin H. Lim[1,2] | Chae Hyun Kim[1,2] | Alexander Sandberg[5] | Chuanwen Fan[5] | Pernille Lauritzen[4] | Henrik Molina[6] | Christopher Peralta[6] | Jacob B. Geri[7] | Colin Burdette[8] | Dai Hoon Han[3] | Heon Yung Gee[9] | Insuk Lee[10] | Jeon-Soo Shin[11] | Hyunwook Kim[1] | Leon Li[4] | Gabriel C. Tobias[4] | Inbal Wortzel[4,12] | Sang Joon Shin[1] | Hyo-Il Jung[13] | Min Goo Lee[8] | Soonmyung Paik[14] | Robert E. Schwartz[15] | Joong Bae Ahn[1] | David Lyden[4] | Han Sang Kim[1,2,4]

[1]Division of Medical Oncology, Department of Internal Medicine, Yonsei Cancer Center, Yonsei University College of Medicine, Seoul, Republic of Korea | [2]Graduate School of Medical Science, Brain Korea 21 FOUR Project, Severance Biomedical Science Institute, Yonsei University College of Medicine, Seoul, Republic of Korea | [3]Division of Colorectal Surgery, Department of Surgery, Yonsei University College of Medicine, Seoul, Republic of Korea | [4]Children's Cancer and Blood Foundation Laboratories, Departments of Pediatrics, and Cell and Developmental Biology, Drukier Institute for Children's Health, Meyer Cancer Center, Weill Cornell Medicine, New York, New York, USA | [5]Department of Clinical and Experimental Medicine, Linköping University, Linköping, Sweden | [6]Proteomics Resource Center, The Rockefeller University, New York, New York, USA | [7]Department of Pharmacology, Weill Cornell Medicine, New York, New York, USA | [8]Tri-Institutional PhD Program in Chemical Biology, Weill Cornell Medicine, New York, New York, USA | [9]Department of Pharmacology, Yonsei University College of Medicine, Seoul, Republic of Korea | [10]Department of Biotechnology, College of Life Science and Biotechnology, Yonsei University, Seoul, Republic of Korea | [11]Department of Microbiology, Brain Korea 21 FOUR Project for Medical Science, Yonsei University College of Medicine, Seoul, Republic of Korea | [12]Department of Cancer Biology and Immunology, Tel-Aviv University, Tel-Aviv, Israel | [13]School of Mechanical Engineering, Yonsei University, Seoul, Republic of Korea | [14]Theragen Bio Co., Ltd, Seongnam-si, South Korea | [15]Division of Gastroenterology and Hepatology, Department of Medicine, Weill Cornell Medicine, New York, New York, USA

Correspondence: David Lyden (dcl2001@med.cornell.edu) | Han Sang Kim (modeerfhs@yuhs.ac)

Received: 4 August 2025 | **Revised:** 19 February 2026 | **Accepted:** 22 March 2026

ABSTRACT

Early detection of colon adenocarcinoma (COAD) remains suboptimal. Fecal tests fail to diagnose 30% of stage I cancer, and serum CEA lacks sensitivity (< 40%). Extracellular vesicles (EVs) circulate systemically and package tumor-related cargo, making them attractive non-invasive biomarkers for cancer diagnosis. We profiled the EV proteome from 233 human patients using LC-MS/MS, including stage I-IV tumors with matched non-tumor colon tissues (n = 50 each; n = 100), paired pre-/post-operative plasma (n = 90) and healthy plasma (n = 43). Circulating EVs contained both tumor-specific and stromal/immune cell-derived proteins, reflecting the systemic nature of EV biology in the cancer setting. Proteomic analysis identified 745 proteins enriched in tumor-derived EVs (e.g., SRPK1, THBS2) and 127 proteins enriched in adjacent tissues. Plasma EVs revealed 166 proteins enriched in COAD (e.g., UBA1, FCN1) and 233 enriched in healthy controls. Pathway analysis linked tumor EV cargo to angiogenesis, mRNA splicing, TGF-β signalling and RNA translation. Notably, a cross-cancer comparison (pancreatic = 10, lung = 14 cases) revealed that 76% of tumor EV proteins were COAD-specific, highlighting tissue of origin specificity. We further developed a 10-protein EV panel comprising seven tumor-associated and three healthy-enriched EV proteins, which effectively distinguished COAD patients from healthy controls in the two validation cohorts (n = 104 and n = 215), achieving > 90% sensitivity for differentiating COAD

Yura Seo, Yoon Dae Han, and Linda Bojmar shared co-first authorship

One Sentence Summary: A 10-protein extracellular-vesicle blood test detects colon cancer earlier and more sensitively than current clinical markers.

from healthy and non-COAD colorectal conditions. Six weeks after curative resection, tumor-associated EV proteins decreased by > 70%, whereas healthy-associated proteins rebounded to baseline, indicating surgical responsiveness. Collectively, EV protein signatures provide a sensitive and tissue-specific window into tumor–host communication, further supporting blood-based early detection of COAD.

1 | Introduction

Early cancer detection is critical for reducing cancer-related mortality (Corcoran and Chabner 2018). Liquid biopsies, which are used to analyse circulating biomarkers, have emerged as a promising tool for early cancer detection, recurrence monitoring and assessment of drug responsiveness (Corcoran and Chabner 2018; Cohen et al. 2018; Jung et al. 2023). Liquid biopsy refers to the minimally invasive sampling and molecular analysis of circulating biofluids, such as circulating tumor DNA (ctDNA), circulating tumor cells and extracellular vesicles (EVs) (Yu et al. 2021; Zhou et al. 2022). This approach offers an alternative to invasive tissue biopsies and facilitates the identification of biomarkers to detect the early stages of cancer. Current research efforts are focused on solid cancers with relatively challenging early diagnoses, including gastrointestinal cancers, such as pancreatic, liver and colorectal carcinomas (Glass and Coffey 2022; Melo et al. 2015; Sun et al. 2023; Nakamura et al. 2022).

Colon adenocarcinoma (COAD) is the third most common cancer and the second leading cause of cancer-related deaths worldwide (Bray et al. 2024). For decades, colonoscopy has been the gold standard for COAD screening, providing direct visualisation of the colon (Dekker et al. 2019). However, this invasive procedure can cause discomfort, bleeding and perforation and has a low adherence rate of approximately 40% (Force et al. 2021; Robertson et al. 2017; Singal et al. 2017). Non-invasive stool-based screening methods, such as the fecal immunochemical test (FIT), high-sensitivity guaiac fecal occult blood test and multitarget stool DNA test (FIT-DNA), have demonstrated varying sensitivity and specificity (Imperiale et al. 2014). FIT has a sensitivity of approximately 74% and specificity of 95%, while FIT-DNA exhibits higher sensitivity at 92% but lower specificity at 87%. Despite these improvements, screening adherence remains suboptimal at approximately 60% (Force et al. 2021; Robertson et al. 2017). Imaging-based approaches, such as positron emission tomography–computed tomography radiomics, are also being investigated for COAD diagnosis, particularly in combination with machine learning techniques (Kim et al. 2023). Blood-based carcinoembryonic antigen (CEA) testing lacks specificity for COAD, with a sensitivity and specificity of 50% and 80%, respectively (Fletcher, 1986; Sorensen et al. 2016). Circulating tumour DNA (ctDNA) assays offer improved specificity, up to 90% in metastatic COAD—but their sensitivity remains limited (~50%) in detecting early-stage or non-metastatic disease, (Cohen et al. 2018; Dasari et al. 2020; Sonpavde et al. 2019; Gupta et al. 2020; Chung et al. 2024) highlighting the urgent need for more reliable circulating biomarkers for COAD.

Growing evidence suggests that EVs are valuable for early cancer detection, prognosis and therapy guidance (Yu et al. 2021; Hoshino et al. 2020; Chen et al. 2017; Shah et al. 2018). EVs are generally classified as microvesicles, exosomes and apoptotic bodies; however, because these labels imply distinct biogenesis pathways that are not always directly demonstrated in most biofluid studies, we use the operational term 'EVs' (and, where appropriate, 'small EV-enriched' preparations) throughout this work. EVs carry nucleic acids, lipids and proteins and can reflect both disease-associated and systemic host responses, making them attractive candidates for liquid biopsy applications (Al-Nedawi et al. 2008; Becker et al. 2016; Skog et al. 2008; Thakur et al. 2014; Wortzel et al. 2024). Circulating EVs are stably released from parental cells at concentrations of up to 10^{10} vesicles/mL, providing material that reflects the systemic status of the body (Hoshino et al. 2020; Johnsen et al. 2019). EVs facilitate intercellular communication by transferring proteins and nucleic acids that can reprogram the tumor microenvironment (TME) and distant organs, influencing cancer development and progression processes, such as the epithelial–mesenchymal transition (EMT), pre-metastatic niche formation and metastasis (Becker et al. 2016; Jeppesen et al. 2014; Costa-Silva et al. 2015). Identifying novel EV biomarkers involved in these processes could improve early cancer detection, prognosis and monitoring for minimal residual disease (Parikh et al. 2021).

Patients with cancer exhibit increased EV production through several mechanisms, such as enhanced oncogenic signalling pathways, and endoplasmic reticulum stress and hypoxia (Kalluri and McAndrews 2023). Most EVs are sourced from primary tumors, the TME, distant organs (e.g., liver) and the immune system (e.g., bone marrow) (Hoshino et al. 2020). Examining cancer-associated EV proteins in the blood, primary colon tumor tissues and adjacent colon tissues will enhance our understanding of tumor-specific and host-responsive protein signatures in cancer development and progression.

In this study, we examined the proteomes of EVs isolated from 190 human samples, including paired tumors and adjacent colon tissues from fresh surgical specimens obtained from patients with newly diagnosed COAD, as well as plasma samples collected pre-operatively (on the day of surgery) and post-operatively (six weeks after surgery). We hypothesised that specific proteins found in EVs from the plasma and colon tissue could serve as reliable, non-invasive biomarkers for the early detection of COAD. We compared plasma-derived EVs from patients with COAD with those from healthy controls and validated the findings using the enzyme-linked immunosorbent assay (ELISA).

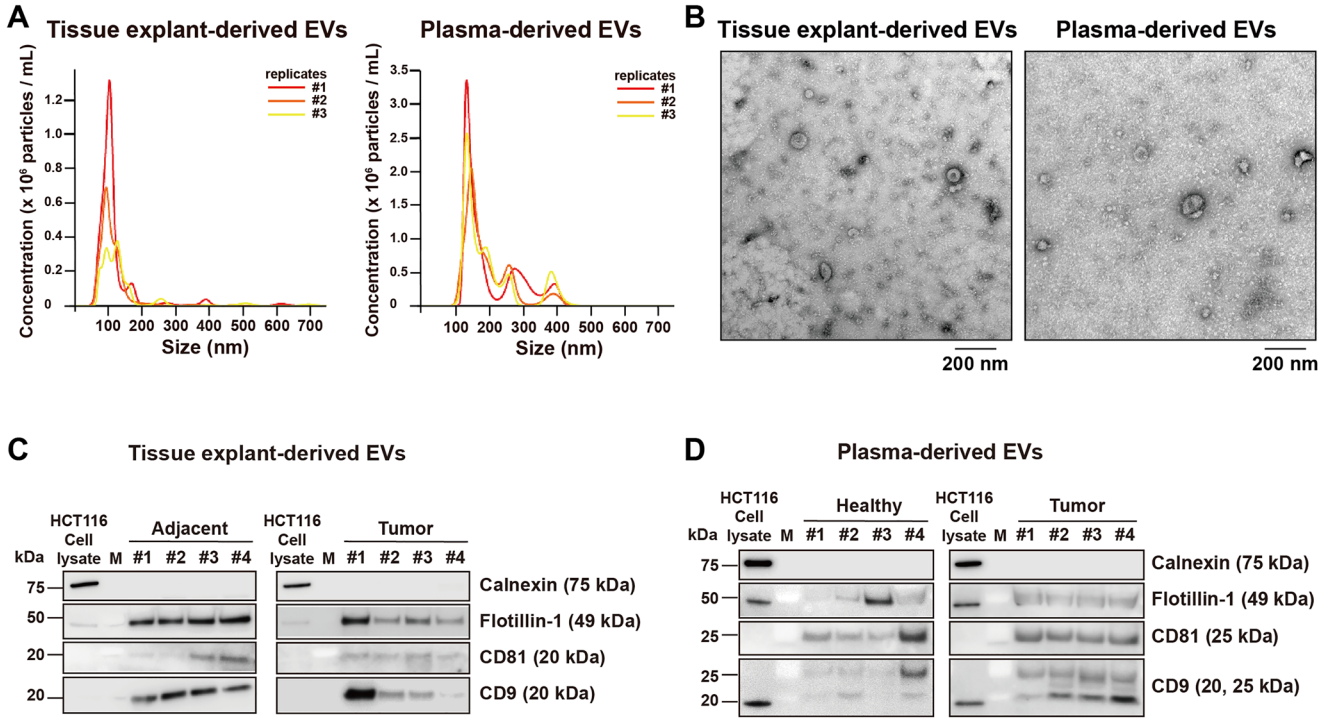

FIGURE 1 | Characterisation of EVs isolated from colon tissue explants and plasma in COAD.

(A) Nanoparticle tracking analysis showing the concentration and size distribution of EVs isolated from human tissue explants and plasma. (B) Transmission electron microscopy images of EVs isolated from human tissue explants and plasma. (C) Immunoblotting of HCT116 cell lysates and EVs isolated from tissue explants (adjacent normal and tumor colon tissues), probed for the negative EV marker calnexin and the positive EV markers flotillin-1, CD81, and CD9. (D) Immunoblotting of HCT116 cell lysates and EVs isolated from plasma of healthy controls and patients with COAD, probed for calnexin, flotillin-1, CD81 and CD9.

M, molecular weight marker.

2 | Results

2.1 | Characterization of EVs Isolated From Colon Tissue Explants and Plasma in COAD

Samples were accrued in two non-overlapping periods: May 2019–September 2022 for the discovery cohort and the 1st EV-ELISA validation cohort and September 2022–January 2025 for an independent 2nd EV-ELISA validation cohort (Table S1). EVs were isolated from tissue explants and plasma using sequential ultracentrifugation (Figure S1). For discovery-stage profiling, we performed LC–MS/MS on EVs from 190 specimens obtained from 92 patients with COAD, including tumor tissues ($n = 50$), matched adjacent tissues ($n = 50$), preoperative plasma ($n = 62$) and post-operative plasma collected six weeks after surgery ($n = 28$). For ELISA-based translation, we assembled a 1st validation cohort ($n = 104$; 84 COAD and 20 healthy controls) and measured 22 candidate EV proteins in plasma EVs (preoperative $n = 84$; paired post-operative $n = 84$; healthy controls $n = 20$) (Figure S2 and Table S1). We then evaluated the finalised EV-10 level using a locked cut-off in an independent 2nd validation cohort ($n = 215$) that additionally included clinically relevant non-COAD colorectal conditions (benign polyp, tubular adenoma with dysplasia and hereditary polyposis syndromes) (Table S1).

To confirm that our preparations were consistent with EV-enriched populations suitable for downstream proteomics and EV-ELISA, we characterised EV size, morphology and marker expression. Nanoparticle tracking analysis (NTA) and transmission electron microscopy (TEM) showed a predominant small EV-sized population, with modal diameters of ~100 nm for tissue explant–derived EVs and ~135 nm for plasma-derived EVs, and overall size distributions largely <150 nm (Figure 1A,B). We further validated EV identity and purity by immunoblotting for canonical EV markers (flotillin-1, CD81 and CD9) and a negative EV marker, calnexin (endoplasmic reticulum (ER) protein), as well as including HCT116 cell lysates as non-EV controls (Figure 1C,D). EV preparations from both tissue explants and plasma were enriched for flotillin-1, CD81 and CD9, while calnexin was undetectable in EV lanes but readily detected in the HCT116 cell lysate control, supporting minimal ER contamination and the integrity of EV-enriched isolates used in subsequent analyses (Figure 1C,D).

2.2 | Identification of Tumor-Specific EV Proteins Released rom the COAD Tissue

To first define tumor-associated EV programs at their source while prioritizing biologically grounded candidates before evaluating circulating EV signals, we profiled tissue-derived EV proteomes from resected COAD tumors and matched adjacent colon tissues (Figure 2 and Figure S2). In the discovery cohort, we analysed EV proteomes from 190 specimens, including colon

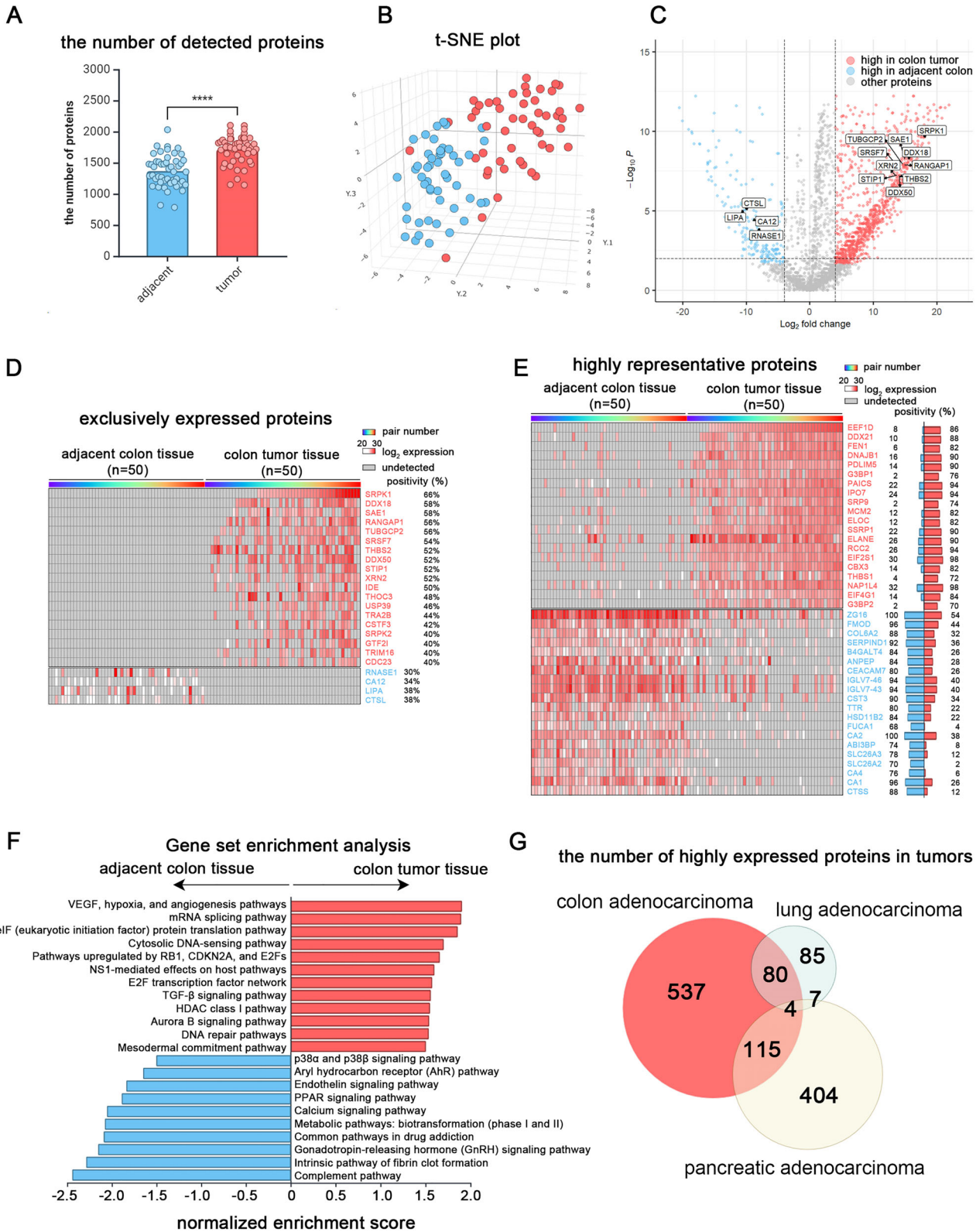

FIGURE 2 | Identification of tumor-specific EV proteins released from the COAD tissue.

(A) Bar graph showing the number of EV proteins detected in colon cancer tissue explants compared with that in adjacent non-tumor colon tissue explants. (B) *t*-distributed stochastic neighbour embedding (*t*-SNE) plot illustrating distinct expression patterns between EVs derived from colon cancer tissues and those from adjacent normal tissues. (C) Volcano plot highlighting the top-enriched EV proteins in colon cancer tissue- versus adjacent tissue-derived EVs. (D) Top exclusively-expressed EV proteins in colon tumor tissues ($n = 50$) and adjacent colon tissues ($n = 50$). (E) Top 20 most-expressed EV proteins in colon tumor tissues ($n = 50$) and adjacent colon tissues ($n = 50$). (F) Top-enriched biological pathways identified by gene set enrichment analysis in EVs from colon tumor tissues (top panel) and adjacent tissues (bottom panel). (G) Venn diagram comparing tumor-associated EV proteins identified in colon, lung, and pancreatic adenocarcinomas.

tumor tissues (n = 50), matched adjacent tissues (n = 50), preoperative plasma (n = 62) and post-operative plasma collected six weeks after surgery (n = 28). The median number of unique proteins detected in EVs derived from colon tumor tissues was 1755 (interquartile 25%–75% range, 1604–1,870), which was significantly higher than the median of 1356 proteins detected in EVs derived from adjacent colon tissues (interquartile 25%–75% range, 1187–1521; $P < 0.0001$; Figure 2A). Protein expression patterns were distinct between the colon cancer and adjacent colon tissues in the *t*-distributed stochastic neighbour embedding plot (Figure 2B). We identified 745 and 127 highly expressed proteins in EVs derived from tumor and adjacent colon tissues, respectively ($\log_2$ fold change > 4-fold; adjusted $P < 0.001$; Figure 2C). The top proteins exclusively expressed in the tumor or adjacent colon tissues or highly representative are highlighted in Figure 2D,E, respectively.

Notably, 19 proteins were exclusively expressed in > 40% of colon tumor samples and were associated with messenger RNA (mRNA) processing (SRSF protein kinase 1 [SRPK1], DEAD-box helicase 18 [DDX18], serine and arginine-rich splicing factor 7 [SRSF7], 5'-3' exoribonuclease 2, THO complex subunit 3, ubiquitin-specific peptidase 39 [USP39], transformer 2 beta homolog [TRA2B], cleavage stimulation factor subunit 3 and SRPK2) (Yi et al. 2018; Saijo et al. 2016; Zhao et al. 2025; Akaike et al. 2014; Xiong et al. 2018), chromosome segregation (SRPK1, USP39, SRPK2, SUMO1 activating enzyme subunit 1, Ran GTPase activating protein 1 [RANGAP1], tubulin gamma complex component 2 and cell division cycle 23) (Wu et al. 2023; Yang et al. 2024; Murphy et al. 1998; Wang et al. 2003), and Rho GTPase signalling (RANGAP1, TRA2B and stress-induced phosphoprotein 1) (Akaike et al. 2014; Yang et al. 2024; Zhang et al. 2018), suggesting that EV proteins reflect the hallmark of colon cancer, such as alternative splicing (Yi et al. 2018; Saijo et al. 2016; Zhao et al. 2025; Akaike et al. 2014; Xiong et al. 2018), genome instability (Wu et al. 2023; Yang et al. 2024; Murphy et al. 1998; Wang et al. 2003), or sustaining proliferative signalling (Akaike et al. 2014; Yang et al. 2024; Zhang et al. 2018) (Figure 2D). By contrast, catabolic enzymes, including cathepsin (CST) L, lipase A, lysosomal acid type, carbonic anhydrase (CA) 12 and pancreatic ribonuclease A family member 1, were exclusively detected in EVs derived from the adjacent colon tissue (Figure 2D). These proteins are commonly expressed in the gastrointestinal tract, as shown in the Human Protein Atlas (Uhlen et al. 2015) and play physiological roles, including pH homeostasis regulation (CA12) (Kivela et al. 2000), digestive ribonuclease activity (RNASE1) (Singh et al. 2025) and lysosomal enzyme functions (LIPA and CTSL) (Zhang 2018).

The top 20 highest-representative proteins, based on the fold change between the adjacent colonic and tumor tissues, are shown in Figure 2E. The most prominent tumor-related proteins linked with stress granules, including G3BP stress granule assembly factors 1 and 2, DDX21, importin 7 (IPO7), flap structure-specific endonuclease 1 (FEN1) and eukaryotic translation initiation factor 2 subunit alpha and 4 gamma 1 (EIF2S1 and EIF4G1). Other translation factors, including EIF2S1, EIF4G1, eukaryotic translation elongation factor 1 delta, signal recognition particle 9, thrombospondin 1 (THBS1) and IPO7 were also observed. Proteins associated with nucleosome assembly included minichromosome maintenance complex component 2, nucleosome assembly protein 1-like 4, structure-specific recognition protein 1 and FEN1. By contrast, highly represented proteins in the adjacent colonic tissues were linked with physiologic colonic function, such as bicarbonate transport (CA4 and solute carrier family 26 members 2 and 3) and adaptive immune response (immunoglobulin lambda variable 7–43 [IGLV7-43], IGLV7-46 and CTSS) (Figure 2E and Table S2). Similar to the restricted protein pathways mentioned above, Gene Set Enrichment Analysis (GSEA) revealed RNA processing pathways and VEGF signalling as the most highly represented pathways in COAD. GSEA also identified tumor-derived EVs as being enriched for pathways associated with hypoxia, angiogenesis and mRNA splicing, the eukaryotic initiation factor protein translation pathway, transforming growth factor-beta (TGF-β) signalling and the cytosolic DNA-sensing pathway, which are crucial for colon cancer development and progression (Figure 2F and Table S3). Conversely, EVs derived from adjacent colonic tissues were primarily associated with the complement pathway (Figure 2F).

To contextualize whether tumor tissue–enriched EV proteins were predominantly colon-specific or instead reflected broader pan-adenocarcinoma programs, we compared colon tumor tissue–derived EV proteins with EV proteomes previously generated from pancreatic and lung adenocarcinoma tissues using the same EV isolation protocol, the same proteomics facility and the same statistical pipeline (Figure 2G and Table S4), (Hoshino et al. 2020). Notably, four proteins—THBS2, splicing factor 3b subunit 3, inosine triphosphatase and four and a half LIM domains 2—were commonly identified across the three cancer types, indicating their potential role as pan-cancer diagnostic biomarkers. Overall, 48% (84/176) of enriched lung tumor tissue–derived EV proteins were also found in colon tumor tissue–derived EVs, whereas 23% (119/530) of pancreatic tumor tissue–derived EV proteins overlapped with those from the colon tumor (Figure 2G). Notably, 73% (537/736) of the identified enriched EV proteins were unique to colon tumors. This indicates that most of the colon tumor derived-EV proteins are specific to the colon tissue, which may assist in identifying tumors of unknown origin in certain patients.

We prioritised tumor tissue–exclusive candidates via EV proteomics, only advancing when plasma EVs were detected preoperatively, and lost after surgery within matched plasma. This is because downstream validation was designed to nominate circulating EV biomarkers measurable from blood. Among the tumor tissue–exclusive proteins that met the selection criteria were, SRPK1 and THBS2. These two proteins were detected in preoperative plasma EVs and were subsequently undetected post-operatively, consistent with a tumor-linked circulating EV signal. In addition, overlap analysis across colon, lung, and pancreatic adenocarcinoma tissue EV datasets identified THBS2 as one of the four proteins shared all three cancer types (Figure 2G and Table S4), supporting broader diagnostic relevance. Accordingly, SRPK1 and THBS2 were carried forward into the EV-ELISA candidate list, whereas the remaining tumor tissue–exclusive proteins were not pursued for plasma ELISA due to limited evidence of detectability in circulation in this discovery dataset.

2.3 | Discovery of Plasma-Derived EV Proteins Detected Only before the Surgical Removal of Tumor Tissues

To identify colon cancer-associated plasma EV proteins, we compared the protein profiles of EVs isolated from preoperative plasma samples ($n = 62$), post-operative plasma samples collected 6 weeks after surgery ($n = 28$), and healthy control plasma samples ($n = 43$; reference plasma EV proteomics dataset from (Hoshino et al. 2020)). Each post-operative plasma sample was paired with its corresponding preoperative sample. The median number of unique proteins detected in plasma-derived EVs was 316 (interquartile range, 242–356), 281 (interquartile range, 259–300) and 311 (interquartile range, 285–336) in preoperative, post-operative and healthy control samples, respectively.

Next, we compared preoperative plasma samples with healthy control samples and identified 166 and 233 highly expressed EV proteins, respectively (log2 fold change > 2-fold, adjusted $P < 0.05$; Figure 3A). Similarly, we compared pre- and post-operative plasma samples and identified 57 and 15 highly expressed EV proteins, respectively (log2 fold change > 2-fold, adjusted $P < 0.05$; Figure 3B). Based on these differential expression analyses, we selected 10 candidate proteins enriched in preoperative plasma samples and those enriched in healthy control samples (Figure 3C). Tumor-associated EV proteins included ficolin-1 (FCN1)—a pattern recognition receptor involved in the innate immune response and activation of the lectin complement pathway—and heterogeneous nuclear ribonucleoprotein K (hnRNPK)—an RNA-binding protein involved in RNA splicing, stability and translation. Additionally, proteins associated with translation, folding, degradation and ubiquitination were identified, such as ribosomal protein SA (RPSA), CTSB, proteasome 20S subunit beta 3 (PSMB3), ubiquitin-like modifier activating enzyme 1 (UBA1), chaperonin containing TCP-1 subunit 8 (CCT8), metabolic enzyme-like esterase D (ESD) and 5-aminoimidazole-4-carboxamide ribonucleotide formyltransferase/IMP cyclohydrolase (ATIC). Furthermore, tumor-associated proteins identified in preoperative plasma-derived EVs were enriched in pathways related to RNA metabolism, amino acid metabolism, protein translation, MYC targets and ribonucleoprotein complex biogenesis (Figure 3D and Table S5). By contrast, enriched EV proteins in healthy controls included soluble pattern recognition receptors (collectin subfamily members 10 [COLEC10] and 11 [COLEC11]), antigen-presenting protein (major histocompatibility complex class I, C [HLA-C]) and proteins associated with the cytoskeleton and cellular movement (ezrin [EZR], alpha-actinin 4 [ACTN4], vasodilator-stimulated phosphoprotein [VASP] and TGF-β induced) (Figure 3C).

We further compared COAD tumor-associated EV proteins with EV proteins previously reported in plasma from pancreatic and lung adenocarcinoma cohorts in order to contextualize these COAD-associated circulating EV proteins relative to other tumor types (Hoshino et al. 2020) (Figure 3E). Notably, proteasome 20S subunit alpha 5 (PSMA5) was identified across all three cancer types. Six proteins (27%; 6/22) derived from lung tumor tissue EVs—PSMB3, CHMP4B, ADARB1, ERN1, ACTR1A and PSMA5—were also detected in colon tumor tissue–derived EVs. Conversely, only 5% (2/43) of pancreatic tumour tissue–derived EV proteins, lactotransferrin and PSMA5, overlapped with those from colon tumours (Figure 3E). Consistent with the tissue-derived analyses, most identified plasma EV proteins (96%, 159/166) were unique to COAD, supporting substantial tissue of origin specificity.

Finally, to interpret whether candidate EV proteins reflect tumor-cell intrinsic secretion versus contributions from the TME or host immune compartments, we next assessed their detectability in EVs derived from colon cancer cell lines (SW620, HT29, HCT116, DLD1 and CT26) (Figure 3F). Notably, some of the tumor-associated plasma EV proteins ($n = 10$; preoperative-enriched), including FCN1 and PSMB3, were not expressed in the tumor cells, suggesting that FCN1 may be released from peripheral blood myeloid cells, such as neutrophils or macrophages, rather than tumor cells themselves (Figure 3F). Similarly, 14 of 39 colon tumor tissue–derived EV proteins were not detected in cancer cell–derived EVs; here, 39 represents the sum of "highly representative" ($n = 20$) and "exclusively expressed" ($n = 19$) tumor tissue–derived EV proteins (Figure 3F). Together, these data suggest that a substantial fraction of COAD-associated EV proteins may originate from non–tumor-cell sources within the TME (e.g., fibroblasts, endothelial cells and immune cells) or systemic host responses.

2.4 | Validation of Plasma-Derived EV Proteins in Patients With COAD and Healthy Controls

Because LC–MS/MS proteomics discovery yields a large set of differentially abundant proteins, we prioritised candidates for follow up ELISA-based assaying using a rationale-driven filter: candidates had to be detectable in plasma EVs, supported by commercially available antibodies and show consistent directionality between discovery and validation settings (Figure S2). We established a 1st EV-ELISA validation cohort comprising 20 healthy controls and 84 patients with COAD. The distribution of cancer stages was as follows—stage I, 18%; stage II, 24%; stage III, 28%; and stage IV, 30%—aligning with that in the discovery cohort (Table S1). We quantified 22 candidate proteins by EV-ELISA, including 12 tumour-associated proteins (SRPK1, THBS2, CHMP4B, CTSB, ESD, CCT8, ATIC, hnRNPK, RPSA, PSMB3, UBA1 and FCN1) and 10 healthy-enriched proteins (COLEC10, COLEC11, RELN, EZR, HLA-C, ACTN4, VASP, DBH, TGFBI and KCTD12) (Figure S2 and Figure S3A).

Candidate retention required both statistical support and concordant directionality relative to discovery (tumor-associated candidates higher in COAD than healthy controls; healthy-enriched candidates higher in healthy controls than COAD). Proteins that did not meet the predefined significance criterion ($P \geq 0.01$) or showed discordant directionality in EV-ELISA were excluded (Figure S3B–C). Based on these criteria (two-sided unpaired t-test; $P < 0.01$), we selected 10 EV proteins for downstream analyses, comprising seven tumor-associated proteins and three healthy control–enriched proteins (Figure S3A).

Among the tumour-associated proteins, UBA1, PSMB3, SRPK1, FCN1, THBS2, ATIC and CCT8 were significantly elevated in

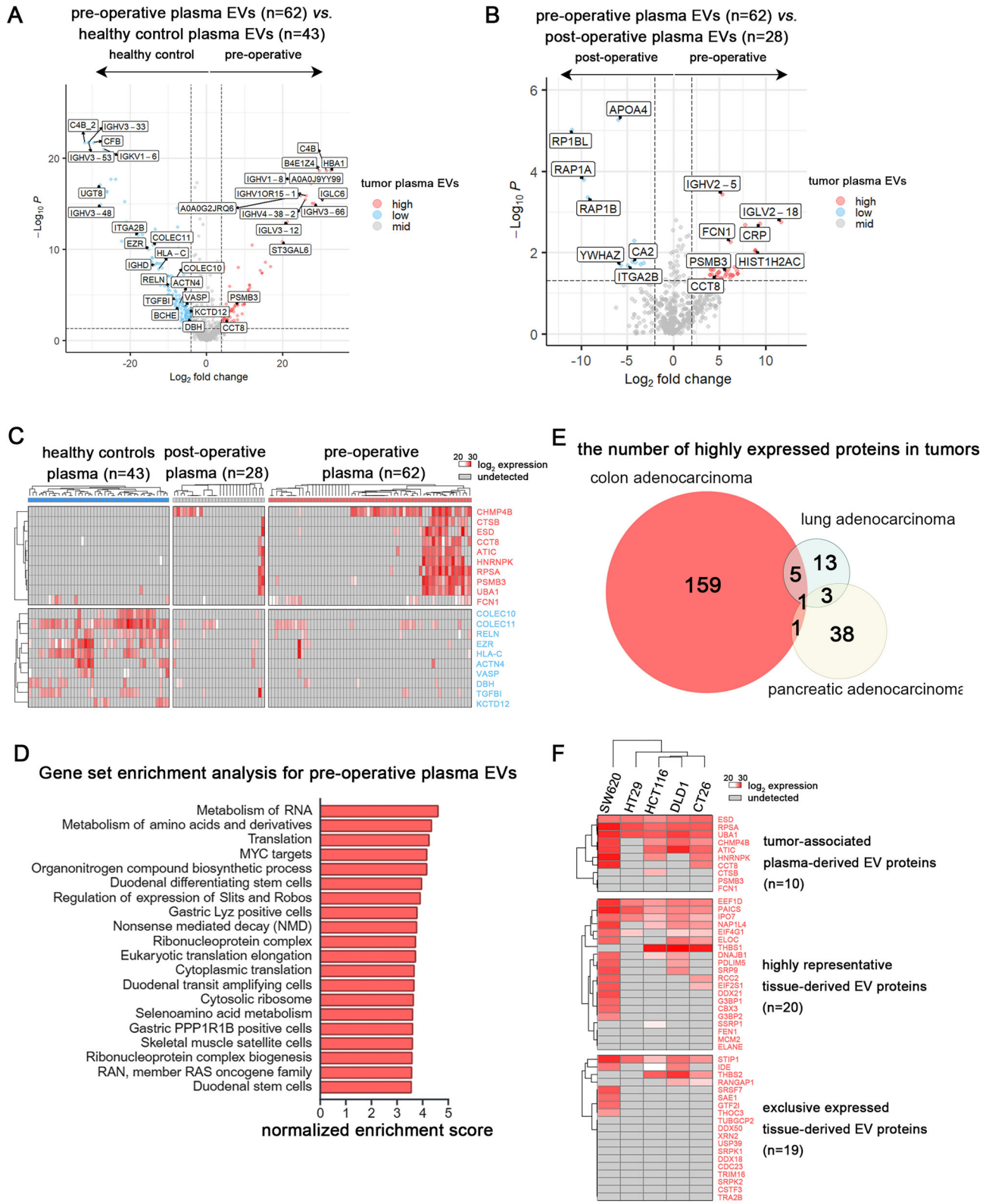

FIGURE 3 | Discovery of plasma-derived EV proteins detected only before the surgical removal of the tumor tissues.
(A) Volcano plot showing the top enriched circulating EV proteins in preoperative colon cancer plasma-derived EVs ($n = 62$) compared with EVs from healthy controls ($n = 43$). (B) Volcano plot highlighting the top enriched circulating EV proteins in preoperative ($n = 62$) versus post-operative ($n = 28$) colon cancer plasma-derived EVs. (C) Heatmap showing the expression of top-candidate EV proteins across pre- ($n = 62$) and post-operative plasma samples from patients with COAD ($n = 28$) and healthy controls ($n = 43$). (D) Top-enriched biological pathways identified by gene set enrichment analysis in EVs from pre-operative plasma EVs. (E) Venn diagram comparing plasma-derived tumor-associated EV proteins identified in colon, lung, and pancreatic adenocarcinomas. (F) Heatmap illustrating the expression patterns of top-enriched EV protein candidates in colon cancer cell lines, including SW620, HT29, HCT116, DLD1 and CT26.

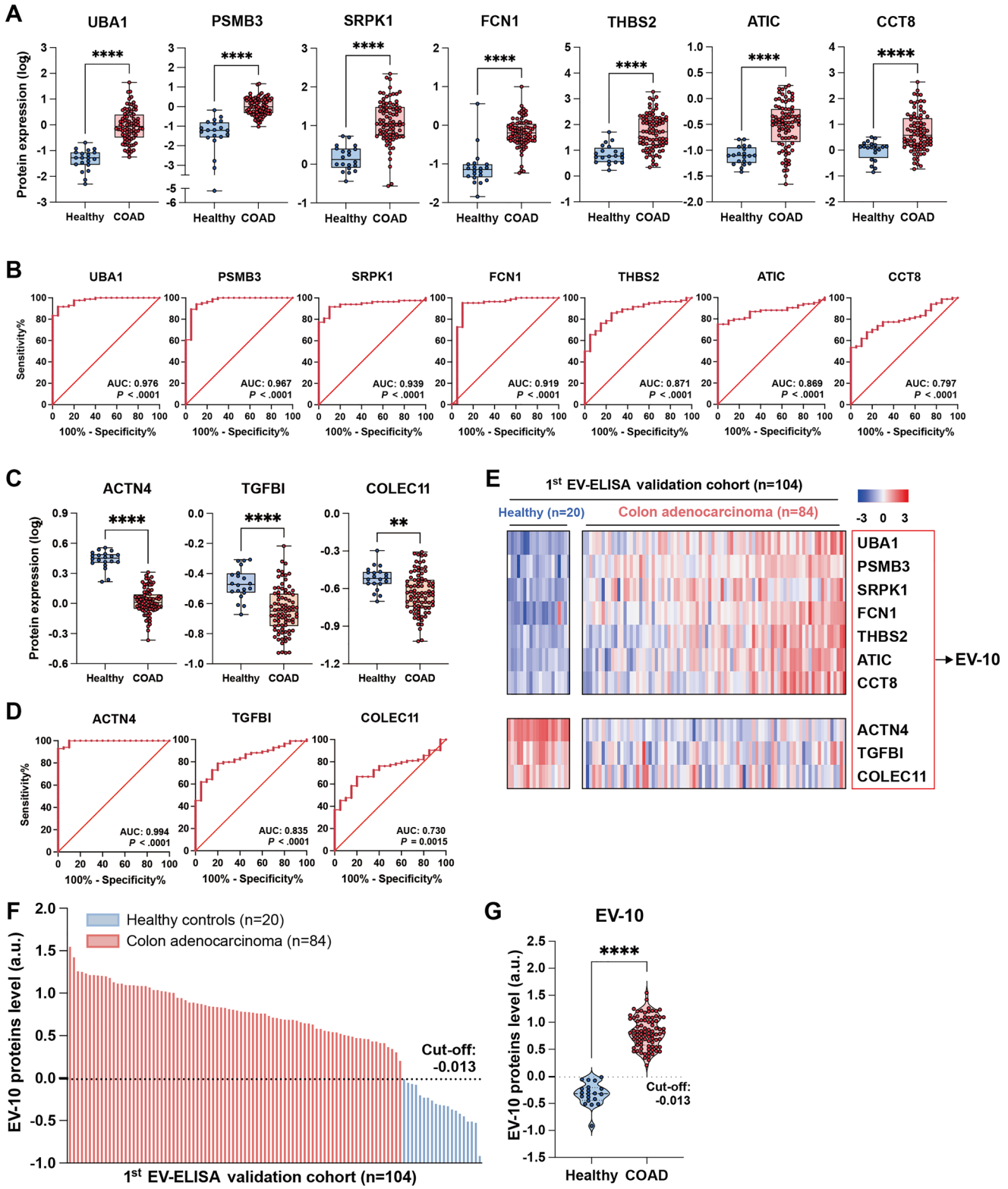

FIGURE 4 | Legend on next page.

patients with COAD compared with healthy controls (two-sided unpaired *t*-test, $P < 0.0001$; Figure 4A). As single markers, these proteins yielded AUCs of 0.797–0.976 (DeLong test, $P < 0.0001$; Figure 4B and Table S6). Similarly, the three healthy control–enriched proteins (ACTN4, TGFBI and COLEC11) were significantly different between groups (two-sided unpaired *t*-tests; $P \leq 0.0015$; Figure 4C), with AUCs ranging from 0.730 to 0.994 (DeLong test; Figure 4D and Table S6).

To improve robustness beyond any single marker, we integrated tumour-associated and healthy-enriched signals into a composite score (EV-10), capturing two opposing axes of discrimination in

a single metric. Specifically, EV-10 was calculated by subtracting the mean expression of the three healthy-enriched proteins from the mean expression of the seven tumour-associated proteins (Figure 4E). Using a cohort-defined threshold of −0.013 (the highest EV-10 value among healthy controls in the 1st cohort), EV-10 values showed clear separation between healthy controls and patients with COAD in this validation set (Figure 4F,G). Together, these results nominate EV-10 as a candidate circulating EV-based biomarker for COAD and motivated locked-threshold evaluation in an independent cohort.

2.5 | Comparison of EV-10 With Serum CEA and Plasma ctDNA and Perioperative Changes After Surgery

To assess the diagnostic utility of EV-10 in the 1st validation cohort, we compared EV-10 with serum CEA and plasma ctDNA. Preoperative CEA was measured before curative-intent surgery, and post-operative CEA was measured 6 weeks after surgery. For ctDNA analysis, 26 patients were randomly selected from the 1st validation cohort (stage I, 19%; stage II, 19%; stage III, 31%; stage IV, 31%). The same preoperative plasma samples used for EV-ELISA were analysed using the Guardant360 CDx assay to detect ctDNA somatic alterations.

Across stages, serum CEA and ctDNA tended to be higher in stage IV compared with earlier stages, although differences were not statistically significant. EV-10 values were elevated in COAD across stages and did not significantly vary by stage (Figure 5A). For detection-rate comparisons, CEA was considered positive at > 5 ng/mL, ctDNA positivity was defined by detection of somatic alterations, and EV-10 positivity was defined as EV-10 > −0.013. In this cohort, EV-10 showed higher observed positivity across stages than CEA and ctDNA (Figure 5B and Figure S4); however, ctDNA was assessed in a limited subset ($n = 26$) and stage-stratified comparisons should be interpreted cautiously. Notably, the stage-invariant EV-10 signal suggests that EV-10 may be more informative for detection than for capturing stage-associated differences. Together, these results suggest that EV-10 may provide complementary diagnostic information to conventional markers.

We next assessed perioperative changes using paired pre- and post-surgery plasma samples ($n = 84$). Serum CEA decreased after surgery (two-sided paired t-test, $P < 0.0001$; Figure 5C). In EV-ELISA, six of seven tumour-associated EV proteins decreased post-operatively (Figure 5D), whereas the three healthy-enriched proteins increased (Figure 5E), resulting in a significant decrease in EV-10 values (two-sided paired t-test, $P < 0.0001$; Figure 5F). Post-operative EV-10 values approached those observed in healthy controls (Figure 5G). Using the same threshold to binarize EV-10 status, EV-10 positivity significantly decreased after surgery (77/84 converted from positive to negative; McNemar's exact test, two-sided $P < 0.0001$; Figure 5F,G).

2.6 | Evaluation in an Independent 2nd EV-ELISA Validation Cohort, Including Non-COAD Colorectal Conditions

For further validation, we tested EV-10 in an independent 2nd EV-ELISA validation cohort ($n = 215$) from the same single-center (Yonsei Cancer Center). This 2nd cohort included healthy controls without colorectal disease ($n = 11$), non-COAD colorectal conditions ($n = 45$; benign polyp $n = 15$; tubular adenoma with dysplasia $n = 25$; hereditary polyposis syndromes $n = 5$), and COAD patients ($n = 159$; stage I $n = 18$, stage II $n = 49$, stage III $n = 56$, stage IV $n = 36$). EV-10 values did not significantly differ among non-COAD subgroups or across COAD stages I–IV. However, EV-10 differed significantly across the three clinical strata (healthy controls vs non-COAD vs COAD) (one-way ANOVA with Tukey's multiple comparisons test, $P < 0.001$; Figure 5H).

We applied the same EV-10 cut-off (−0.013) defined in the 1st cohort to the independent 2nd cohort. Using this fixed threshold, EV-10 classification (Healthy + non-COAD, $n = 56$ vs COAD, $n = 159$) was significantly associated with disease status (Fisher's exact test, $P < 0.0001$; Figure 5I). ROC analyses further assessed separation between (i) Healthy and each non-COAD condition (Figure 5J) and (ii) pooled non-COAD conditions and COAD by stage (Figure 5K), demonstrating strong discrimination between COAD and non-COAD conditions while remaining largely stage-invariant.

Together, LC–MS/MS screening in the discovery cohort identified 22 candidate EV proteins, which were subsequently evaluated by plasma EV-ELISA in the 1st validation cohort and refined to a 10-protein EV-10 panel. A threshold derived from healthy controls in the 1st cohort was then locked and applied to an independent 2nd cohort that included clinically relevant non-COAD colorectal conditions. Across these analyses, EV-10 distinguished

FIGURE 4 | Validation of tumour biomarkers using plasma-derived EVs from patients with COAD and healthy controls.
(A) ELISA analysis of seven tumour-associated proteins in EVs isolated from the plasma, comparing healthy controls and patients with COAD. Error bars represent the median with interquartile range. P values were calculated using a two-sided unpaired t-test. (B) ROC curve analysis using the DeLong test for the proteins shown in (A). (C) ELISA analysis of three proteins enriched in plasma-derived EVs from healthy controls compared with those derived from patients with COAD. Error bars represent the median with interquartile range. P values were calculated using a two-sided unpaired t-test. (D) ROC curve analysis using the DeLong test for the proteins shown in (C). (E) Heatmap showing the relative expression of proteins from (A) and (C). Each protein expression value is standardised (Z-score). A new biomarker, EV-10, is defined by subtracting the average expression of the three healthy control-associated proteins from that of the seven tumour-associated proteins. (F) Waterfall plot of EV-10 protein levels. Using a cutoff value of −0.013 (the highest value among healthy controls), patients with COAD and healthy controls are clearly separated. Values are shown in arbitrary units (a.u.), calculated by subtracting the average expression of the three healthy control-enriched proteins from the seven tumour-associated proteins. (G) Comparison of EV-10 protein levels between healthy controls and patients with COAD based on the cutoff value of −0.013. Values are shown in a.u. P value was calculated using a two-sided unpaired t-test. Data are shown as individual points with summary statistics as plotted. Statistical significance is indicated as ns, $P < 0.05$, *$P < 0.01$, **$P < 0.001$, ***$P < 0.0001$.

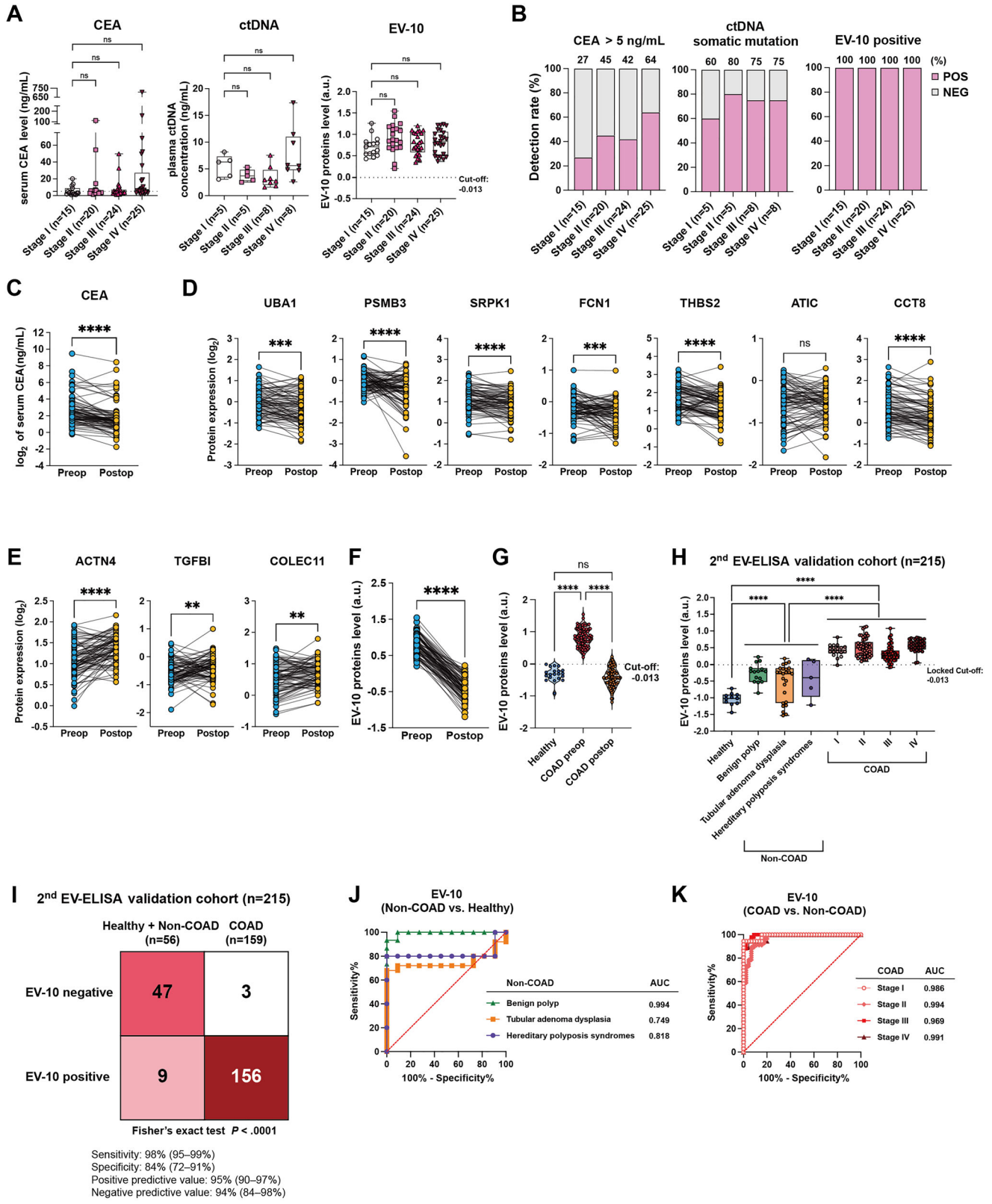

FIGURE 5 | Legend on next page.

COAD from cancer-free groups and decreased after curative-intent surgery. These findings support further evaluation of EV-10 in larger, independent multi-center cohorts and in combination with existing modalities, such as CEA and ctDNA.

3 | Discussion

This study identified 10 EV proteins derived from colon tissues and plasma as potential diagnostic biomarkers for COAD. These

circulating biomarkers, enriched in the plasma of patients with COAD and healthy controls, were validated in an independent cohort and showed higher sensitivity than serum CEA and ctDNA analyses. Following surgery, tumor-derived EV protein levels decreased, whereas healthy EV protein levels increased, further supporting their diagnostic potential for COAD. These COAD-specific proteins were distinct from those associated with other types of cancer. Collectively, our findings underscore the potential of EV proteins in the liquid biopsy for the diagnosis of COAD.

The EV-based detection rate for early stages I–II was higher than that of conventional serum CEA or plasma ctDNA (Figure 5). Cancer is a systemic disease that can alter the cargo of EVs originating from cancer cells, immune cells, and other organs. Although serum CEA and plasma ctDNA are primarily derived from tumor cells, the advantage of using EV proteins in the liquid biopsy is their ability to provide insights into the interactions between cancer and the body, offering systemic information. Our proteomic analysis encompasses both colon tissue–derived EVs and circulating EVs in the plasma to assess whether circulating proteins are also detectable in colon tissues. Notably, SRPK1 and THBS2 were present in colon cancer tissue–derived EVs but were absent in adjacent colon tissue–derived EVs, suggesting that these proteins likely originate from the colon cancer tissue microenvironment. However, other circulating EV biomarkers, such as ATIC, PSMB3, CCT8 and UBA1 were not identified in colon cancer tissue–derived EVs, indicating that these proteins are more likely derived from immune cells or other organs. Notably, we observed that EV proteins associated with innate immune response (e.g., FCN1 and COLEC11) and metabolic enzymes (e.g., ESD and ATIC) were altered in COAD. These altered EV proteins may interfere with antitumor immunity, potentially affecting M2 macrophage polarization (Tkach et al. 2022) and neutrophil extracellular traps (Su et al. 2023). Alternatively, they may contribute to the metabolic reprogramming of distant cells, such as endothelial cells, (Harmati et al. 2021) thereby enhancing premetastatic niche formation or distant metastasis during cancer development and progression (Becker et al. 2016).

Notably, several top-enriched proteins in tumor tissue explant–derived EVs appear to play a role in intercellular communication within the TME, particularly in modulating VEGF signalling, mRNA splicing and TGF-β signalling, as revealed by pathway analysis. One of the most notable proteins identified in our dataset was the extracellular matrix protein THBS2. THBS2 has also been significantly detected in pancreatic and lung adenocarcinomas. THBS2 expression is linked to cancer-associated fibroblast (CAF) activation, the TGF-β pathway, and EMT activation within the immunosuppressed TME (Bagaev et al. 2021; Thorsson et al. 2018). Our findings showed that THBS2 expression is lower than that of THBS1 in colorectal cancer cell lines, with predominant expression observed in CAFs, as indicated by a single-cell RNA sequencing dataset (Zhou et al. 2024). These data suggest that CAF-derived THBS2 is a characteristic feature of colorectal cancer tissue–derived and circulating EVs. However, the mechanism by which THBS2 in CAF-derived EVs impacts tumor cells, immune cells, or other TME components, and its specific role within the local TME remains elusive. Targeting these interactions may provide new opportunities for developing targeted treatment strategies against the TME. Moreover, the role of circulating EV-derived THBS2 in the formation of premetastatic niches in distant organs, such as the liver, is yet to be fully understood. Another notable group of proteins includes translation initiation factors, such as EIF2S1 and EIF4G1, as well as the splicing factor SRPK1. The recipient cells and the underlying mechanisms through which EVs transport these proteins and associated mRNA, which can then be translated into recipient cells to regulate gene expression and protein synthesis, are not yet fully understood within the TME. A better understanding of these intercellular communication processes could offer valuable insights into tumor development and inform potential strategies for targeting the TME.

In the context of cancer biomarker identification, comparing tissue-derived and circulating EVs has highlighted important distinctions with potential clinical relevance, such as whether the proteins are sourced from primary tumours or distant organs. Among the EV-10 proteins, THBS2, (Hoshino et al. 2020) ATIC, (Chang et al. 2021) and CCT8 (Cho et al. 2021) have been previously reported as potential circulating biomarkers for cancer, which supports our findings. However, discrepancies in circulating EV protein biomarkers have been observed across studies. These inconsistencies could be attributed to factors, such as heterogeneous study populations (e.g., variations in cancer stages, race, and inclusion of healthy participants), differences in sample preparation (e.g., plasma vs. serum), variability in EV

FIGURE 5 | Comparison of the diagnostic accuracy of EV-10 with conventional biomarkers and the prognostic value of EV-10 before and after surgery.

(A) Serum CEA, plasma ctDNA concentration and EV-10 level across COAD stages (CEA and EV-10: stage I $n = 15$, stage II $n = 20$, stage III $n = 24$, stage IV $n = 25$; ctDNA: stage I $n = 5$, stage II $n = 5$, stage III $n = 8$, stage IV $n = 8$). (B) Detection rates by stage for CEA (> 5 ng/mL), ctDNA somatic mutation detection and EV-10 positivity (EV-10 ≥ -0.013; negative if EV-10 < -0.013) using the same locked cut-off. Data are presented as percentages of positive diagnoses across stages I–IV. (C–F) Pre- and post-surgery comparison of (C) serum CEA levels, (D) seven tumour-associated proteins, (E) three healthy control-enriched proteins, and (F) EV-10 levels in patients with COAD. *P* values were calculated using a two-sided paired *t*-test. (G) EV-10 levels in healthy controls and in patients with COAD pre- and post-operatively; the locked cut-off (−0.013) is indicated by a dotted line. (H) EV-10 scores in the 2nd EV-ELISA validation cohort. The EV-10 cut-off (−0.013) defined in the 1st validation cohort was applied unchanged. Group differences were assessed by one-way ANOVA with Tukey's multiple-comparisons test (healthy vs. non-COAD vs. COAD). (I) Confusion matrix summarising EV-10 classification in the 2nd validation cohort (healthy controls or benign condition, $n = 56$ vs. COAD, $n = 159$) using the locked cut-off (−0.013) and the same positivity definition as in (B). *P*-value was calculated by a two-sided Fisher's exact test. (J) ROC curves of EV-10 for distinguishing non-COAD colorectal conditions (benign polyp, tubular adenoma with dysplasia and hereditary polyposis syndromes) from healthy controls (healthy as the reference). AUCs are shown in the panel. (K) ROC curves of EV-10 for distinguishing COAD (stage I–IV) from non-COAD colorectal conditions (pooled) (non-COAD as the reference). Stage-specific AUCs are shown in the panel. Data are shown as individual points with summary statistics as plotted. Statistical significance is indicated as ns, $P < 0.05$, $^{*}P < 0.01$, $^{**}P < 0.001$, $^{***}P < 0.0001$.

isolation techniques (e.g., differential ultracentrifugation vs. size-exclusion chromatography), and variations in protein analysis methods (e.g., LC-MS/MS vs. ELISA) (Vergauwen et al. 2017). Standardization of protein detection methods, larger prospective validations and the evaluation of protein detection across different platforms are essential for refining biomarker discovery in EV-based cancer diagnosis.

Current CRC screening guidelines recommend screening average-risk adults beginning at age 45 using established stool-based tests and direct visualization tests, with individualised decisions beyond age 75. Because our cohorts were not designed as a prospective, average-risk screening study, EV-10 may not be interpreted as a replacement for colonoscopy or FIT. Rather, our data support EV-10 as a complementary EV-based biomarker with two near-term potential applications: (i) perioperative monitoring following curative-intent surgery, supported by paired pre/post reductions in EV-10 levels and positivity, and (ii) an adjunctive tool to support diagnostic evaluation and triage, particularly when used in combination with existing biomarkers, such as CEA and ctDNA. Although ctDNA was available only in a small subset of the 1st validation cohort, exploratory paired analyses suggested that EV-10 may relate to ctDNA somatic mutation detection in non-metastatic disease, supporting potential complementarity between a systemic EV-proteomic signal (EV-10) and mutation-level characterization by ctDNA. Larger paired cohorts will be required to validate integrated approaches and quantify incremental value.

Based on this study, future directions include identifying EV proteins with prognostic significance. EV diagnostic proteins are not necessarily the same as those with prognostic impact. Although diagnostic proteins are likely involved in the initial development of tumors, prognostic proteins may play a role in cancer metastasis and treatment resistance. Additionally, comparing EV proteins derived from the primary colon cancer tissue with those from metastatic tissues (e.g., liver or lung) could uncover novel proteins that help elucidate organotropic EV proteins. Targeting these organotropic EV proteins could facilitate multiorgan therapies, such as addressing thrombosis in the lung or preventing dysregulated metabolism in the liver (Lucotti et al. 2025; Wang et al. 2023). Comparing EV proteomes from colon cancer organoids, normal colon organoids and current colon tissue–derived EVs could enhance our understanding of EV proteomes, helping identify which EV proteins are cancer-specific or TME-specific. Finally, deeper proteomic coverage may improve detection of low-abundance proteins and further refine EV biology, for example, through longer liquid chromatography gradients, data-independent acquisition, and/or newer platforms, such as timsTOF, while maintaining an appropriate balance between throughput and clinical feasibility.

This study has several limitations. First, age/sex distributions differed between the discovery-stage reference controls and the YCC COAD discovery cohort (Table S1). Although EV-10 was subsequently evaluated in validation cohorts with comparable age/sex distributions using a locked cut-off, residual confounding at the discovery stage cannot be fully excluded. In the 2nd validation cohort, a modest sex imbalance remained between cancer-free controls and COAD (Table S1), which should be considered when interpreting performance estimates. Second, the sample size is insufficient to generalize our findings, and the retrospective nature of the study necessitates future prospective validation using larger cohorts. Third, ELISA relies on commercially available antibodies, limiting our ability to test all potentially valuable proteins; high-throughput platforms (e.g., proximity extension assay) may improve scalability. Fourth, although we included an independent cohort with clinically relevant non-COAD colorectal conditions, we did not evaluate EV-10 in a prospective average-risk screening population. Therefore, EV-10 performance for population-level screening or as a substitute for guideline-recommended screening tools (FIT/colonoscopy) remains unknown. Moreover, while we did not include inflammatory intestinal conditions (e.g., inflammatory bowel disease) or other inflammation/microbiome-associated states, investigating these conditions in future studies will be important to further define the clinical specificity of EV-10. Finally, prospective multicenter external validation will be required to establish broader generalizability.

In conclusion, we characterised the proteomes of colon tissue–derived and circulating EVs from patients with COAD and cancer-free controls and validated an EV-10 protein panel as a candidate non-invasive biomarker to support COAD detection and clinical evaluation (Figure S5).

4 | Materials and Methods

4.1 | Study Design

This study aimed to identify and validate diagnostic EV protein biomarkers for COAD using patient-derived tissue and plasma samples. All samples were collected at Yonsei Cancer Center (YCC, single-center only). Samples were accrued in two non-overlapping periods: May 2019–September 2022 for the discovery LC–MS/MS and 1st EV-ELISA validation cohorts and September 2022–January 2025 for the independent 2nd EV-ELISA validation cohort. In the discovery cohort (COAD, $n = 92$), EVs were isolated from resected tumour tissue, matched adjacent normal tissue and available matched pre- and post-operative plasma, followed by LC–MS/MS proteomic profiling to nominate candidate markers (Table S1). Candidate proteins were then evaluated by EV-ELISA in a 1st validation cohort comprising healthy controls without colorectal disease ($n = 20$) and patients with COAD (preoperative, $n = 84$) with paired post-operative plasma samples collected 6 weeks after surgery ($n = 84$), to refine a 10-protein panel (EV-10). A cohort-defined cut-off (−0.013; the highest EV-10 value among healthy controls in the 1st cohort) was pre-specified and subsequently applied unchanged to an independent 2nd EV-ELISA validation cohort ($n = 215$) comprising healthy controls without colorectal disease ($n = 11$), non-COAD colorectal conditions (benign polyp, tubular adenoma with dysplasia, hereditary polyposis syndromes; $n = 45$) and COAD ($n = 159$), to assess performance against clinically relevant cancer-free colorectal conditions. Diagnostic performance was compared with pre-operative serum CEA ($n = 84$ in the 1st cohort) and plasma ctDNA (Guardant360 CDx) measured in a subset of the same preoperative plasma samples (available for patients with COAD in the 1st cohort, $n = 26$). Sample sizes were determined by specimen availability.

4.2 | Human Specimen Preparation and Processing

Tumor and adjacent fresh colon tissues and plasma samples were obtained from patients treated at YCC between May 2019 and January 2025. All COAD cases were pathologically confirmed. Preoperative plasma was collected prior to curative-intent surgery and post-operative plasma was collected six6 weeks after surgery. Healthy control plasma samples were obtained from individuals without a history of malignancy and without colorectal disease (no COAD or polyps confirmed by colonoscopy). The 2nd EV-ELISA validation cohort additionally included patients with non-COAD colorectal conditions (benign polyp, tubular adenoma with dysplasia and hereditary polyposis syndromes), as detailed in Table S1. For discovery-stage plasma EV proteomics, healthy control reference data ($n = 43$) were obtained from a previously published dataset (Hoshino et al. 2020) (Table S1). All participants provided written informed consent under a protocol approved by the Institutional Review Board of Severance Hospital, Yonsei University College of Medicine (IRB no. 4-2019-0811), and the study was conducted in accordance with the Declaration of Helsinki. Clinical information, including age, sex, tumor histology and tumor stage (American Joint Committee on Cancer staging system 8th edition), was collected (Table S1).

Colon tissue samples were processed as previously described (Bojmar et al. 2021). In brief, fresh tumors and adjacent colon tissues located 4 cm away from the cancer site were harvested from patients with COAD undergoing resection with curative intent at YCC. The tissue was placed in ice-cold phosphate-buffered saline (PBS) within minutes of collection and submitted for downstream processing and analysis. The tissues were cut into small pieces and cultured for 7–14 h in the serum-free Roswell Park Memorial Institute medium, supplemented with penicillin (100 U/mL) and streptomycin (100 μg/mL).

Plasma samples were collected from patients with COAD and from healthy controls with no history of COAD or polyps, as confirmed by colonoscopy, as previously described (Bojmar et al. 2021). Sample volumes varied from 2–4 mL of plasma. Blood samples collected in lavender-top EDTA tubes were kept at room temperature for 10 min, followed by centrifugation at 1900×g for 15 min (Figure S1). The obtained supernatant was aliquoted and stored at −80°C; a subset of preoperative plasma samples ($n = 26$) was submitted for ctDNA profiling (Guardant360 CDx), and the remaining plasma was processed for EV isolation (Figure S1).

4.3 | Cell Lines and Cell Culture

CT26, DLD-1, SW620, HCT116 and HT29 cell lines were cultured in DMEM, supplemented with penicillin (100 U/ml), streptomycin (100 mg/ml) and 10% fetal bovine serum (FBS). Mycoplasma testing was performed before EV isolation for all cell lines using the American Type Culture Collection (ATCC) Mycoplasma Testing Kit. All cells were maintained in a humidified incubator with 5% CO_2 at 37°C and were routinely tested and confirmed to be free of mycoplasma contamination. When collecting conditioned media for EV isolation, FBS (GIBCO, Thermo Fisher Scientific, Waltham, MA) was first depleted of EVs by ultracentrifugation at 100,000 × g for 70 min. Cells were cultured for 3–4 days, and supernatant was collected before the cells reached confluency (Bojmar et al. 2021).

4.4 | EV Purification, Characterization and Analyses

EVs were purified by sequential ultracentrifugation, as previously described (Bojmar et al. 2021). Briefly, plasma, resected tissue culture supernatant, or cell line culture media were centrifuged at 500 × g for 10 min to remove cells. To remove dead cell, apoptotic bodies and large cell debris, the supernatants were centrifuged at 3000 × g for 20 min, followed by centrifugation at 12,000 × g for 20 min to eliminate large microvesicles. Finally, EVs were collected by centrifuging at 100,000 × g for 70 min. EVs were washed in PBS and pelleted again by ultracentrifugation at 100,000 × g for 70 min using a Beckman Coulter Optima XE or XPE ultracentrifuge (Figure S1). The final EV pellet was resuspended in 200 μL of PBS and stored at −80°C. Protein concentration was measured using a BCA assay (Pierce, Thermo Fisher Scientific, Waltham, MA). The NS300 nanoparticle characterization system (NanoSight, Malvern Instruments, Malvern, UK) analysed EV size and particle number with a red laser (642 nm). the histograms represent three individual replicates, with the experiment performed at least three times. Plasma-derived EVs at a concentration of 5000 μg/ml were diluted at a ratio of 1:2000, while tissue explant-derived EVs at a concentration of 1000 μg/ml were also diluted at a ratio of 1:2000.

4.5 | Transmission Electron Microscopy (TEM)

For negative staining TEM analysis, a solution containing 0.1 μg/μl of EVs in PBS was applied onto a grid coated with formvar and carbon (Bojmar et al. 2024). The EVs were allowed to settle on the grid for 1 min. The specimen was then blotted and treated with four consecutive drops of 1.5% aqueous uranyl acetate, with blotting performed after each drop. After the final stain application, the grid was blotted and allowed to dry naturally. The grids were observed using a JEOL JEM-1400 transmission electron microscope (JEOL USA Inc., Peabody, MA), operated at a voltage of 100 kV. Images were captured using a Veleta 2K × 2K CCD camera (Olympus-SIS, Munich, Germany).

4.6 | Western Blot Analysis

A total of 20 μg of EV protein extracts from tissue explants was used for western blot analysis. And, a total of 50 μg of EV protein extracts from plasma was used. And a total of 10 μg of cell lysate protein extracts from cell lysate was used. Cell lysate and EVs were lysed using RIPA lysis and extraction buffer (Thermo Fisher Scientific, Waltham, MA), supplemented with 1X protease inhibitor cocktail and phenylmethylsulfonyl fluoride (Sigma-Aldrich, Burlington, MA). Sonication was performed to enhance protein lysis. The denatured proteins were mixed with NuPAGE LDS Sample Buffer (Invitrogen, Thermo Fisher Scientific, Waltham, MA) and β-mercaptoethanol, then heated at 95°C for 5 min. Proteins were separated by electrophoresis on 4%–12% Bolt BISTRIS Plus gels (Invitrogen, Thermo Fisher Scientific, catalog number TFS-NW04120BOX, Waltham, MA)

and transferred onto polyvinylidene difluoride membranes using iBlot 2 Transfer Stacks (Invitrogen, Thermo Fisher Scientific, catalog number TFS-IB24002, Waltham, MA).

The membranes were blocked with 1X PBS containing 5% skim milk (w/v) and 0.1% Tween-20 (v/v), then incubated overnight at 4°C with the primary antibodies. All primary antibodies were diluted at 1:1000 in a blocking buffer. The membranes were washed three times with 1X PBS containing 0.1% Tween-20 (v/v), incubated with horseradish peroxidase (HRP)-conjugated secondary antibodies and washed three more times to remove unbound antibodies. Immunoblots were visualised using Super-Signal West Femto Maximum Sensitivity Substrate (Thermo Fisher Scientific, catalog number 34095, Waltham, MA) and ImageQuant LAS4000 mini (GE Healthcare, Chicago, IL). A list of all antibodies used is provided in Table S7.

4.7 | Liquid Chromatography-Tandem Mass Spectrometry (LC-MS/MS)

LC-MS/MS proteomic analysis was performed as previously described (Hoshino et al. 2020; Bojmar et al. 2024). In brief, EV protein samples were first dried using a vacuum centrifuge. Proteins were denatured in 8 M urea prepared in 50 mM ammonium bicarbonate (AMBIC) (Sigma, catalog number 09839), reduced with 10 mM dithiothreitol (Millipore sigma, catalog number 233156) and alkylated using 100 μM iodoacetamide (Sigma, catalog number I1149) in 50 mM AMBIC under light-protected conditions. Samples were sequentially digested with LysC (for 4–5 h) followed by overnight trypsin (Prometa, catalog number V5111) digestion at 37°C. Proteolysis was terminated by acidification with trifluoroacetic acid, and peptides were cleaned using solid-phase extraction on C18 stage tips (CDS, catalog number 2215). Elution was performed with 70% acetonitrile containing 0.1% trifluoroacetic acid (Sigma, catalog number 302031), followed by vacuum drying and resuspension in 2% acetonitrile in water. Peptides analysed at the Rockefeller University Proteomics Core following established Core procedures (Hoshino et al. 2020; Bojmar et al. 2024). Approximately 3 μg of peptide from each sample was analysed by high-resolution nano–LC–MS/MS using reversed-phase C18 separation at 200 nL/min with a linear gradient (typically 90 min) from 1% to 35% buffer B (buffer A: 0.1% formic acid; buffer B: 0.1% formic acid in 80% acetonitrile). Data were acquired in data-dependent acquisition (DDA) mode in positive-ion polarity on an Orbitrap platform (Thermo Scientific).

4.8 | Proteomic Data Analysis

Raw LC–MS/MS data were searched against the UniProt human proteome database using Proteome Discoverer 1.4 and Mascot 2.4, with peptide-spectrum matches filtered to a 1% false discovery rate. Proteins were quantified using the average area of the three most abundant peptides per protein. Software tools used were open source R packages (https://www.r-project.org, v3.5.0), in which "limma" was used for QC, analysis and exploration of proteomic expression data. For proteins identified by multiple UniProt IDs, values were collapsed using the probe with the maximum intensity. For frequency analysis, proteins were classified as detected or not detected across all samples. Exclusive biomarkers were identified based on the detection criteria in specific sample groups. Biomarker selection was conducted using the Wilcoxon rank-sum test. In GSEA, the entire proteomic expression dataset and MSigDB v5.1 gene sets with default parameters were used to identify significantly enriched sets.

4.9 | EVELISA

EV-ELISA was performed to detect proteins within the EVs (Hoshino et al. 2020). Briefly, 1.5 μg of EVs were resuspended in 0.4 M carbonate buffer and incubated overnight at 4°C on a 96-well plate. The EVs were then washed three times for 5 min with 1 × PBS and permeabilised with 1 × PBS containing 0.2% Triton-X100 (v/v). The plates were blocked with 1 × PBS containing 2% bovine serum albumin (w/v), washed twice for 5 min with 1 × PBS, and incubated overnight at 4°C with the primary antibodies. All primary antibodies were diluted at 1:100–1:500 in a blocking buffer. After washing the plate four times for 5 min with 1 × PBS, it was incubated for 2 h with HRP–conjugated secondary antibodies diluted at 1:1000–1:2000. The plate was washed four more times for 5 min each to remove unbound antibodies. Next, 3,3′,5,5′-tetramethylbenzidine liquid substrate (catalog number T0440, St. Louis, MO) was added and reacted with HRP for 15–30 min. After the colour developed, the reaction was terminated with a stop solution (Thermo Fisher Scientific, catalog number TFS-SS04). Absorbance at 450 nm was measured using a plate reader. All antibodies used are listed in Table S7. All EV-ELISA experiments using the same samples and antibodies were conducted on the same plate to minimize potential batch effects. Each experiment was performed twice to ensure consistent and reproducible results. Proteins were excluded if they were undetectable in plasma or lacked commercially available antibodies.

4.10 | EV-ELISA Data Analysis

For the EV-ELISA, 1.5 μg of EVs were used to coat each well. To account for variations in the amount of EVs across the samples, we measured the optical density at 450 nm for three tetraspanin proteins: CD81, CD9 and CD63. The expression levels of these three proteins were averaged to serve as the normalization standard for each EV sample. All subsequent candidate protein optical densities were normalised by dividing them by this average and $\log_2$-transformed, and the results were labelled as "protein expression ($\log_2$)". For the EV-10 score, the mean expression of the seven tumor-associated proteins was subtracted by the mean expression of the three healthy-enriched proteins. The EV-10 cut-off (−0.013) was defined in the 1st EV-ELISA validation cohort (n = 104) as the highest EV-10 value among healthy controls, and this threshold was subsequently applied as a pre-specified (locked) cut-off in the independent 2nd EV-ELISA validation cohort (n = 215).

4.11 | Plasma ctDNA Somatic Mutation Test

The Guardant360 CDx Blood Collection Kit was used for this analysis. Blood samples were collected in lavender-top EDTA tubes, kept at room temperature for 10 min and then centrifuged

at 1900 × g for 15 min. The supernatant, the plasma sample, was partially stored at −80°C for ctDNA analysis. A total of 4 mL of plasma was shipped to the Guardant Health Clinical Laboratory, located in Redwood City, CA, USA. ctDNA extraction, library preparation, enrichment and DNA sequencing were performed from each plasma sample. The analysis focused on Single Nucleotide Variants (SNVs) and Insertions and Deletions (Indels) across a panel of 74 select genes, followed by data analysis and reporting.

4.12 | Statistical Analysis

Statistical analyses were conducted using R software (https://www.r-project.org, v3.5.0) or GraphPad Prism (v9.4.1). Statistical significance was assessed using a two-tailed Student's *t*-test, Wilcoxon rank-sum test, or two-way analysis of variance for multiple comparisons with the Sidak method. The results are presented as means ± standard error of the mean. In biological experiments, a *P*-value of < 0.05 was considered statistically significant. A false discovery rate of < 0.05 after multiple comparison corrections was considered statistically significant for proteomics data analysis. The levels of statistical significance are denoted as follows: $*P < 0.05$, $**P < 0.01$, $***P < 0.001$, $****P < 0.0001$.

The performance of the EV protein panel in distinguishing between patients with COAD and healthy controls was assessed using the area under the ROC curve (AUC). Changes in EV protein levels between pre- and post-operative samples were analysed to determine whether these proteins could serve as biomarkers for COAD detection. Statistical significance was determined using paired *t*-tests or nonparametric equivalents to compare protein levels between the groups. Proteins that were undetectable in the plasma or lacked commercially available antibodies were excluded from the analysis. All data points were used for the remaining proteins, and no missing values existed in the final analysis. The sample size was determined based on the expected differences in EV protein levels between patients with COAD and healthy controls, as well as between pre- and post-operative plasma samples. We aimed to detect significant differences in EV protein levels with a power of 0.8 (80% probability of detecting a true difference) and an alpha level of 0.05 (5% chance of a type I error).

Author Contributions

Yura Seo: methodology, validation, investigation, visualization, writing – original draft, writing – review and editing. **Yoon Dae Han**: investigation, resources. **Linda Bojmar**: methodology. **Kyung-A Kim**: formal analysis. **Yurin Seo**: formal analysis. **Taeyul K. Kim**: formal analysis. **Suho Lee**: formal analysis. **Yeleem Kim**: formal analysis. **Hye Bin Choi**: formal analysis. **Yujin H. Lim**: formal analysis. **Chae Hyun Kim**: formal analysis. **Alexander Sandberg**: formal analysis. **Chuanwen Fan**: formal analysis. **Pernille Lauritzen**: methodology. **Henrik Molina**: methodology, software. **Christopher Peralta**: software. **Jacob B. Geri**: software. **Colin Burdette**: software. **Dai Hoon Han**: resources. **Heon Yung Gee**: resources. **Insuk Lee**: investigation. **Jeon-Soo Shin**: investigation. **Hyunwook Kim**: resources. **Leon Li**: resources. **Gabriel C. Tobias**: resources. **Inbal Wortzel**: resources. **Sang Joon Shin**: investigation. **Hyo-Il Jung**: investigation. **Min Goo Lee**: investigation. **Soonmyung Paik**: investigation. **Robert E. Schwartz**: resources. **Joong Bae Ahn**: resources. **David Lyden**: conceptualization, writing – review and editing, supervision. **Han Sang Kim**: conceptualization, visualization, writing – original draft, writing – review and editing, supervision, project administration.

Acknowledgements

The authors gratefully acknowledge support from the following funding sources: National Research Foundation of Korea (NRF) grants 2022R1A2C4001879 (H.S.K.), 2022M3A9F3016364 (H.S.K.), and RS-2026-25469803 (H.S.K.); the Korea Health Technology R&D Project through the Korea Health Industry Development Institute (KHIDI), funded by the Ministry of Health & Welfare, Republic of Korea, grants HI22C0353 (H.S.K.), RS-2023-00304686 (H.S.K.), RS-2025-25459033 (H.S.K.), RS-2025-25459146 (H.S.K.), and RS-2023-00261820 (J.B.A.); the "Hankookilbo Myung-Ho Seung" Faculty Research Assistance Program of Yonsei University College of Medicine grant 6-2023-0172 (H.S.K.); Institute for Project-Y funded by Yonsei University (H.S.K.); the CKDBiO-YONSEI Microbiome Research Center (CYMRC) research grant (H.S.K.); "The Alchemist Project" through the Ministry of Trade, Industry and Energy (MOTIE, Korea) grant 20012443 (H.S.K.); and National Institutes of Health (NIH) grant T32 GM136640-Tan (C.B.).

Conflicts of Interest

D.L. is on the scientific advisory board of Aufbau Holdings, Ltd. D.L. receives research grant support from Aufbau/Sonder Research X and Atossa Therapeutics.

Data Availability Statement

The data that support the findings of this study are available from the corresponding author upon reasonable request.

References

Akaike, Y., K. Masuda, Y. Kuwano, et al. 2014. "HuR Regulates Alternative Splicing of the TRA2beta Gene in Human Colon Cancer Cells Under Oxidative Stress." *Molecular and Cellular Biology* 34, no. 15: 2857–2873.

Al-Nedawi, K., B. Meehan, J. Micallef, et al. 2008. "Intercellular Transfer of the Oncogenic Receptor EGFRvIII by Microvesicles Derived From Tumour Cells." *Nature Cell Biology* 10, no. 5: 619–624.

Bagaev, A., N. Kotlov, K. Nomie, et al. 2021. "Conserved Pan-Cancer Microenvironment Subtypes Predict Response to Immunotherapy." *Cancer Cell* 39, no. 6: 845–865.e7.

Becker, A., B. K. Thakur, J. M. Weiss, et al. 2016. "Extracellular Vesicles in Cancer: Cell-to-Cell Mediators of Metastasis." *Cancer Cell* 30, no. 6: 836–848.

Bojmar, L., H. S. Kim, K. Sugiura, et al. 2024. "Protocol for Cross-Platform Characterization of Human and Murine Extracellular Vesicles and Particles." *STAR Protocols* 5, no. 1: 102754.

Bojmar, L., H. S. Kim, G. C. Tobias, et al. 2021. "Extracellular Vesicle and Particle Isolation From Human and Murine Cell Lines, Tissues, and Bodily Fluids." *STAR Protocols* 2, no. 1: 100225.

Bray, F., M. Laversanne, H. Sung, et al. 2024. "Global Cancer Statistics 2022: GLOBOCAN Estimates of Incidence and Mortality Worldwide for 36 Cancers in 185 Countries." *CA: A Cancer Journal for Clinicians* 74, no. 3: 229–263.

Chang, L. C., Y. C. Hsu, H. M. Chiu, et al. 2021. "Exploration of the Proteomic Landscape of Small Extracellular Vesicles in Serum as Biomarkers for Early Detection of Colorectal Neoplasia." *Frontiers in Oncology* 11: 732743.

Chen, I. H., L. Xue, C. C. Hsu, et al. 2017. "Phosphoproteins in Extracellular Vesicles as Candidate Markers for Breast Cancer." *Proceedings of the National Academy of Sciences* 114, no. 12: 3175–3180.

Cho, H. J., G. O. Baek, M. G. Yoon, et al. 2021. "Overexpressed Proteins in HCC Cell-Derived Exosomes, CCT8, and Cofilin-1 are Potential Biomarkers for Patients With HCC." *Diagnostics (Basel)* 11, no. 7: 1221.

Chung, D. C., D. M. Gray, H. Singh, et al. 2024. "A Cell-Free DNA Blood-Based Test for Colorectal Cancer Screening." *New England Journal of Medicine* 390, no. 11: 973–983.

Cohen, J. D., L. Li, Y. Wang, et al. 2018. "Detection and Localization of Surgically Resectable Cancers With a Multi-Analyte Blood Test." *Science* 359, no. 6378: 926–930.

Corcoran, R. B., and B. A Chabner. 2018. "Application of Cell-Free DNA Analysis to Cancer Treatment." *New England Journal of Medicine* 379, no. 18: 1754–1765.

Costa-Silva, B., N. M. Aiello, A. J. Ocean, et al. 2015. "Pancreatic Cancer Exosomes Initiate Pre-Metastatic Niche Formation in the Liver." *Nature Cell Biology* 17, no. 6: 816–826.

Dasari, A., V. K. Morris, C. J. Allegra, et al. 2020. "ctDNA Applications and Integration in Colorectal Cancer: An NCI Colon and Rectal-Anal Task Forces Whitepaper." *Nature Reviews Clinical Oncology* 17, no. 12: 757–770.

Dekker, E., P. J. Tanis, J. L. A. Vleugels, et al. 2019. "Colorectal Cancer." *Lancet* 394, no. 10207: 1467–1480.

Fletcher, R. H. 1986. "Carcinoembryonic Antigen." *Annals of Internal Medicine* 104, no. 1: 66–73.

Force, U., K. W. Davidson, M. J. Barry, et al. 2021. "Screening for Colorectal Cancer: US Preventive Services Task Force Recommendation Statement." *Journal of the American Medical Association* 325, no. 19: 1965–1977.

Glass, S. E., and R. J Coffey. 2022. "Recent Advances in the Study of Extracellular Vesicles in Colorectal Cancer." *Gastroenterology* 163, no. 5: 1188–1197.

Gupta, R., T. Othman, C. Chen, et al. 2020. "Guardant360 Circulating Tumor DNA Assay is Concordant With FoundationOne Next-Generation Sequencing in Detecting Actionable Driver Mutations in Anti-EGFR Naive Metastatic Colorectal Cancer." *The Oncologist* 25, no. 3: 235–243.

Harmati, M., M. Bukva, T. Boroczky, et al. 2021. "The Role of the Metabolite Cargo of Extracellular Vesicles in Tumor Progression." *Cancer and Metastasis Reviews* 40, no. 4: 1203–1221.

Hoshino, A., H. S. Kim, L. Bojmar, et al. 2020. "Extracellular Vesicle and Particle Biomarkers Define Multiple Human Cancers." *Cell* 182, no. 4: 1044–1061.e18.

Imperiale, T. F., D. F. Ransohoff, S. H. Itzkowitz, et al. 2014. "Multitarget Stool DNA Testing for Colorectal-Cancer Screening." *New England Journal of Medicine* 370, no. 14: 1287–1297.

Jeppesen, D. K., A. Nawrocki, S. G. Jensen, et al. 2014. "Quantitative Proteomics of Fractionated Membrane and Lumen Exosome Proteins From Isogenic Metastatic and Nonmetastatic Bladder Cancer Cells Reveal Differential Expression of EMT Factors." *Proteomics* 14, no. 6: 699–712.

Johnsen, K. B., J. M. Gudbergsson, T. L. Andresen, et al. 2019. "What is the Blood Concentration of Extracellular Vesicles? Implications for the Use of Extracellular Vesicles as Blood-Borne Biomarkers of Cancer." *Biochimica et Biophysica Acta (BBA) - Reviews on Cancer* 1871, no. 1: 109–116.

Jung, S. H., C. K. Lee, W. S. Kwon, et al. 2023. "Monitoring the Outcomes of Systemic Chemotherapy Including Immune Checkpoint Inhibitor for HER2-Positive Metastatic Gastric Cancer by Liquid Biopsy." *Yonsei Medical Journal* 64, no. 9: 531–540.

Kalluri, R., and K. M McAndrews. 2023. "The Role of Extracellular Vesicles in Cancer." *Cell* 186, no. 8: 1610–1626.

Kim, S., J. H. Lee, E. J. Park, et al. 2023. "Prediction of Microsatellite Instability in Colorectal Cancer Using a Machine Learning Model Based on PET/CT Radiomics." *Yonsei Medical Journal* 64, no. 5: 320–326.

Kivela, A., S. Parkkila, J. Saarnio, et al. 2000. "Expression of a Novel Transmembrane Carbonic Anhydrase Isozyme XII in Normal Human Gut and Colorectal Tumors." *American Journal of Pathology* 156, no. 2: 577–584.

Lucotti, S., Y. Ogitani, C. M. Kenific, et al. 2025. "Extracellular Vesicles From the Lung Pro-Thrombotic Niche Drive Cancer-Associated Thrombosis and Metastasis via Integrin Beta 2." *Cell* 188, no. 6: 1642–1661.e24.

Melo, S. A., L. B. Luecke, C. Kahlert, et al. 2015. "Glypican-1 Identifies Cancer Exosomes and Detects Early Pancreatic Cancer." *Nature* 523, no. 7559: 177–182.

Murphy, S. M., L. Urbani, and T. Stearns. 1998. "The Mammalian Gamma-Tubulin Complex Contains Homologues of the Yeast Spindle Pole Body Components spc97p and spc98p." *Journal of Cell Biology* 141, no. 3: 663–674.

Nakamura, K., Z. Zhu, S. Roy, et al. 2022. "An Exosome-Based Transcriptomic Signature for Noninvasive, Early Detection of Patients With Pancreatic Ductal Adenocarcinoma: A Multicenter Cohort Study." *Gastroenterology* 163, no. 5: 1252–1266e1252.

Parikh, A. R., E. E. Van Seventer, G. Siravegna, et al. 2021. "Minimal Residual Disease Detection Using a Plasma-Only Circulating Tumor DNA Assay in Patients With Colorectal Cancer." *Clinical Cancer Research* 27, no. 20: 5586–5594.

Robertson, D. J., J. K. Lee, C. R. Boland, et al. 2017. "Recommendations on Fecal Immunochemical Testing to Screen for Colorectal Neoplasia: A Consensus Statement by the US Multi-Society Task Force on Colorectal Cancer." *Gastroenterology* 152, no. 5: 1217–1237.e13.

Saijo, S., Y. Kuwano, K. Masuda, et al. 2016. "Serine/Arginine-Rich Splicing Factor 7 Regulates p21-Dependent Growth Arrest in Colon Cancer Cells." *Journal of Medical Investigation* 63, no. 3–4: 219–226.

Shah, R., T. Patel, and J. E Freedman. 2018. "Circulating Extracellular Vesicles in Human Disease." *New England Journal of Medicine* 379, no. 22: 2180–2181.

Singal, A. G., S. Gupta, C. S. Skinner, et al. 2017. "Effect of Colonoscopy Outreach vs Fecal Immunochemical Test Outreach on Colorectal Cancer Screening Completion: A Randomized Clinical Trial." *Journal of the American Medical Association* 318, no. 9: 806–815.

Singh, R., A. Archibald, X. L. Li, et al. 2025. "Identification of a Novel Intracellular Function of the Secreted Ribonuclease RNASE1 in Inhibiting Gene Expression." *Molecular and Cellular Biology* 45, no. 8: 315–326.

Skog, J., T. Wurdinger, S. van Rijn, et al. 2008. "Glioblastoma Microvesicles Transport RNA and Proteins That Promote Tumour Growth and Provide Diagnostic Biomarkers." *Nature Cell Biology* 10, no. 12: 1470–1476.

Sonpavde, G., N. Agarwal, G. R. Pond, et al. 2019. "Circulating Tumor DNA Alterations in Patients With Metastatic Castration-Resistant Prostate Cancer." *Cancer* 125, no. 9: 1459–1469.

Sorensen, C. G., W. K. Karlsson, H. C. Pommergaard, et al. 2016. "The Diagnostic Accuracy of Carcinoembryonic Antigen to Detect Colorectal Cancer Recurrence—A Systematic Review." *International Journal of Surgery* 25: 134–144.

Su, X., A. Brassard, A. Bartolomucci, et al. 2023. "Tumour Extracellular Vesicles Induce Neutrophil Extracellular Traps to Promote Lymph Node Metastasis." *Journal of Extracellular Vesicles* 12, no. 8: e12341.

Sun, N., C. Zhang, Y. T. Lee, et al. 2023. "HCC EV ECG Score: An Extracellular Vesicle-Based Protein Assay for Detection of Early-Stage Hepatocellular Carcinoma." *Hepatology* 77, no. 3: 774–788.

Thakur, B. K., H. Zhang, A. Becker, et al. 2014. "Double-Stranded DNA in Exosomes: A Novel Biomarker in Cancer Detection." *Cell Research* 24, no. 6: 766–769.

Thorsson, V., D. L. Gibbs, S. D. Brown, et al. 2018. "The Immune Landscape of Cancer." *Immunity* 48, no. 4: 812–830e814.

Tkach, M., J. Thalmensi, E. Timperi, et al. 2022. "Extracellular Vesicles From Triple Negative Breast Cancer Promote Pro-Inflammatory Macrophages Associated With Better Clinical Outcome." *Proceedings of the National Academy of Sciences* 119, no. 17: e2107394119.

Uhlen, M., L. Fagerberg, B. M. Hallstrom, et al. 2015. "Proteomics. Tissue-Based Map of the Human Proteome." *Science* 347, no. 6220: 1260419.

Vergauwen, G., B. Dhondt, J. Van Deun, et al. 2017. "Confounding Factors of Ultrafiltration and Protein Analysis in Extracellular Vesicle Research." *Scientific Reports* 7, no. 1: 2704.

Wang, G., J. Li, L. Bojmar, et al. 2023. "Tumour Extracellular Vesicles and Particles Induce Liver Metabolic Dysfunction." *Nature* 618, no. 7964: 374–382.

Wang, Q., C. Moyret-Lalle, F. Couzon, et al. 2003. "Alterations of Anaphase-Promoting Complex Genes in Human Colon Cancer Cells." *Oncogene* 22, no. 10: 1486–1490.

Wortzel, I., Y. Seo, I. Akano, et al. 2024. "Unique Structural Configuration of EV-DNA Primes Kupffer Cell-Mediated Antitumor Immunity to Prevent Metastatic Progression." *Nature Cancer* 5, no. 12: 1815–1833.

Wu, Y. J., S. T. Huang, Y. H. Chang, et al. 2023. "SUMO-Activating Enzyme Subunit 1 is Associated With Poor Prognosis, Tumor Progression, and Radio-Resistance in Colorectal Cancer." *Current Issues in Molecular Biology* 45, no. 10: 8013–8026.

Xiong, Y., Y. Deng, K. Wang, et al. 2018. "Profiles of Alternative Splicing in Colorectal Cancer and Their Clinical Significance: A Study Based on Large-Scale Sequencing Data." *EBioMedicine* 36: 183–195.

Yang, R., C. Yang, D. Su, et al. 2024. "METTL3-Mediated RanGAP1 Promotes Colorectal Cancer Progression Through the MAPK Pathway by Recruiting YTHDF1." *Cancer Gene Therapy* 31, no. 4: 562–573.

Yi, N., M. Xiao, F. Jiang, et al. 2018. "SRPK1 is a Poor Prognostic Indicator and a Novel Potential Therapeutic Target for Human Colorectal Cancer." *Onco Targets Ther* 11: 5359–5370.

Yu, W., J. Hurley, D. Roberts, et al. 2021. "Exosome-Based Liquid Biopsies in Cancer: Opportunities and Challenges." *Annals of Oncology* 32, no. 4: 466–477.

Zhang, H. 2018. "Lysosomal Acid Lipase and Lipid Metabolism: New Mechanisms, New Questions, and New Therapies." *Current Opinion in Lipidology* 29, no. 3: 218–223.

Zhang, Z., H. Ren, L. Yang, et al. 2018. "Aberrant Expression of Stress-Induced Phosphoprotein 1 in Colorectal Cancer and its Clinicopathologic Significance." *Human Pathology* 79: 135–143.

Zhao, Q., J. Zhang, X. Cui, et al. 2025. "A Pan-Cancer Analysis of the Oncogenic and Immunological Roles of THOC3 in Human Cancer." *Scientific Reports* 15, no. 1: 36240.

Zhou, H., L. Zhu, J. Song, et al. 2022. "Liquid Biopsy at the Frontier of Detection, Prognosis and Progression Monitoring in Colorectal Cancer." *Molecular Cancer* 21, no. 1: 86.

Zhou, X., J. Han, A. Zuo, et al. 2024. "THBS2 + Cancer-Associated Fibroblasts Promote EMT Leading to Oxaliplatin Resistance via COL8A1-Mediated PI3K/AKT Activation in Colorectal cancer." *Molecular cancer* 23, no. 1: 282.

Supporting Information

Additional supporting information can be found online in the Supporting Information section.

Supporting Information: jev270278-sup-0001-SuppMat.docx